

We perform the calculation a third time using $\Delta\bar{T}_A$ at all locations and times of year. In this case, the result for 1990–2100 for SUL is 109 mm, GHG 149 mm, almost 20% less in each case than from the first method. This is because $\Delta\bar{T}_A$ is less than the local temperature change for most glaciers, as the warming is generally larger over land than sea, and is greater in northern high latitudes.

Most of the water on land resides in the Greenland and Antarctic ice sheets, but the uncertainty about their state of mass balance is as large as the current observed rate of sea-level rise. However, it is relevant to consider the perturbations that might arise from anthropogenic climate change.

The Greenland ice sheet is similar to other high-latitude ice caps in that increased ablation will be the dominant effect of climate change on the mass balance. Therefore we extend the glacier model by defining four additional regions to cover Greenland, corresponding to different climate regimes¹³. They give a total sea-level rise of 76 mm for 1990–2100 in SUL, 93 mm in GHG. This is only about half the size of the glacier melt in each case (Fig. 3), despite the vastly greater area of the ice sheet, because its high latitude and altitude mean that its average surface temperature will remain low. Expressed as a temperature sensitivity, the contribution from Greenland to sea-level rise is $0.35 \text{ mm yr}^{-1} \text{ K}^{-1}$ in SUL and $0.30 \text{ mm yr}^{-1} \text{ K}^{-1}$ in GHG. Various other estimates¹ have been made of this sensitivity, mostly lying within a range of $0.30 \pm 0.15 \text{ mm yr}^{-1} \text{ K}^{-1}$, an uncertainty of 50%. As with mountain glaciers, we find that the total is increased by the use of $\Delta\bar{T}_A$, but reduced with $\Delta\bar{T}_A$.

The Antarctic ice sheet experiences little ablation in either the current or future climates. Accumulation is mainly balanced by calving of icebergs, at a rate which is unlikely to change substantially over the next century, because it responds on the long timescale of ice-sheet dynamics. But precipitation over Antarctica apparently increases strongly with temperature, so climate change in Antarctica will make a negative contribution to sea level, as a consequence of the greater accumulation which will occur in a warmer climate. The sensitivity has been estimated¹ as $-0.30 \pm 0.15 \text{ mm yr}^{-1} \text{ K}^{-1}$, which would result in a sea-level fall of 79 mm over 1990–2100 with the temperature changes predicted by SUL, roughly cancelling the contribution from Greenland, as other studies have also suggested¹⁴. □

Received 7 April; accepted 18 November 1997.

1. Warrick, R. A., Le Provost, C., Meier, M. F., Oerlemans, J. & Woodworth, P. L. in *Climate Change 1995. The Science of Climate Change* (eds Houghton, J. T. et al.) 359–406 (Cambridge Univ. Press, 1996).
2. Johns, T. C. et al. The second Hadley Centre coupled ocean–atmosphere GCM: Model description, spinup and validation. *Clim. Dyn.* **13**, 103–134 (1997).
3. Mitchell, J. F. B., Johns, T. C., Gregory, J. M. & Tett, S. F. B. Climate response to increasing levels of greenhouse gases and sulphate aerosols. *Nature* **376**, 501–504 (1995).
4. Oerlemans, J. in *Ice in the Climate System* (ed. Peltier, W. R.) (Springer, Berlin, 1993).
5. Zuo, Z. & Oerlemans, J. Contribution of glacier melt to sea level rise since AD 1865: a regionally differentiated calculation. *Clim. Dyn.* **13**, 835–845 (1997).
6. Kattenberg, A. et al. in *Climate Change 1995. The Science of Climate Change* (eds Houghton, J. T. et al.) 285–358 (Cambridge Univ. Press, 1996).
7. Oerlemans, J. & Fortuin, J. P. F. Sensitivity of glaciers and small ice caps to greenhouse warming. *Science* **258**, 115–117 (1992).
8. Oerlemans, J. A model for the surface balance of ice masses: Part I: Alpine glaciers. *Z. Gletscherkunde Glazialgeol.* **27/28**, 63–83 (1991).
9. Oerlemans, J. et al. Modelling the response of glaciers to climate warming. *Clim. Dyn.* (in the press).
10. Meier, M. F. Contribution of small glaciers to global sea level. *Science* **226**, 1418–1421 (1984).
11. Ingram, W. J., Wilson, C. A. & Mitchell, J. F. B. Modeling climate change: an assessment of sea ice and surface albedo feedbacks. *J. Geophys. Res.* **94**, 8609–8622 (1989).
12. Mitchell, J. F. B., Manabe, S., Meleshko, V. & Tokioka, T. in *Climate Change: The IPCC Scientific Assessment* (eds Houghton, J. T., Jenkins, G. J. & Ephraums, J. J.) 131–172 (Cambridge Univ. Press, 1990).
13. Oerlemans, J. The mass balance of the Greenland ice sheet: sensitivity to climate change as revealed by energy-balance modelling. *The Holocene* **1**, 40–49 (1991).
14. Thompson, S. L. & Pollard, D. Greenland and Antarctic mass balances for present and doubled atmospheric CO₂ from the GENESIS version-2 global climate model. *J. Clim.* **10**, 871–899 (1997).
15. Leggett, J., Pepper, W. J. & Swart, R. J. in *Climate Change 1992: The Supplementary Report of the IPCC Scientific Assessment* (eds Houghton, J. T., Callander, B. A. & Varney, S. K.) 69–96 (Cambridge Univ. Press, 1992).

Acknowledgements. R. L. H. Essery, W. J. Ingram and J. F. B. Mitchell made useful comments on the manuscript. J. A. Lowe helped with the calculation of thermal expansion. This work was partly supported by the UK Department of the Environment.

Correspondence should be addressed to J.G. (e-mail: jmgregory@meto.gov.uk).

Oceanic signals in observed motions of the Earth's pole of rotation

Rui M. Ponte*, Detlef Stammer† & John Marshall†

* *Atmospheric and Environmental Research, Inc., 840 Memorial Drive, Cambridge, Massachusetts 02139, USA*

† *Department of Earth, Atmospheric, and Planetary Sciences, Massachusetts Institute of Technology, Cambridge, Massachusetts 02139, USA*

Motion of the Earth's pole of rotation relative to its crust, commonly referred to as polar motion, can be excited by a variety of geophysical mechanisms¹. In particular, changes in atmospheric wind and mass fields have been linked to polar motion over a wide range of timescales, but substantial discrepancies remain between the atmospheric and geodetic observations^{1–4}. Here we present results from a nearly global ocean model which indicate that oceanic circulation and mass-field variability play important roles in the excitation of seasonal to fortnightly polar motion. The joint oceanic and atmospheric excitation provides a better agreement with the observed polar motion than atmospheric excitation alone. Geodetic measurements may therefore be used to provide a global consistency check on the quality of simulated large-scale oceanic fields.

Measurements collected through a variety of observational techniques have firmly established the existence of a wide spectrum of variability in the motion of the Earth's pole. Our planet as a whole conserves its angular momentum except for the known effects of external torques associated with lunisolar tides. Thus, the observed variability in polar motion, measured in the reference frame of the crust and mantle to which instruments are attached, results from angular-momentum exchanges between the mantle and the other main components of the Earth's dynamic system, including the atmosphere and the oceans. The changes in the angular momentum of the last two components may be associated with changes in either their mass fields, hence altering their moments of inertia, or their motion fields relative to the crust. Relevant for polar motion are the changes in the angular-momentum components about the two equatorial axes⁵—conventionally taken to point towards the Greenwich and 90° E meridians.

Taking advantage of the quality of available atmospheric operational analysis systems—which involve the combination of global atmospheric data sets and state-of-the-art numerical models to achieve an optimal estimation of the three-dimensional atmospheric state every 6 or 12 hours—a number of studies^{1–4} have established a clear relation between variable wind and mass fields and polar motion, for seasonal and shorter timescales. The correlation between atmospheric and geodetic time series, though significant, was however far from perfect, and most studies have suggested the potential importance of other sources of excitation, with the oceans being considered prime candidates.

Early attempts at determining the role of the ocean in the excitation of seasonal polar motion^{6,7}, based on models with simplified dynamics, very coarse resolution, no ocean-bottom relief, and limited geographical extent, were necessarily inconclusive because of the nature of the simplifying modelling assumptions. In the past decade, however, ocean modelling has progressed immensely, due to improvements in model formulation, external atmospheric forcing field, and computing power. Although an ocean operational analysis system equivalent to those available for the atmosphere has yet to be developed, several global ocean modelling efforts are currently underway. Recently, general circulation models based on full dynamics and thermodynamics have been reported to

yield non-negligible signals in oceanic angular momentum about the equatorial axes^{8,9}, when compared to the atmosphere. Similar results have also been obtained with a simple constant-density ocean model¹⁰. In that study, the addition of oceanic to atmospheric time series provided some improvement in the coherence with the observed polar motion, mainly at submonthly timescales, but the short extent of the period analysed (~1 year) prevented a more general link between changes in ocean flow and mass fields and polar motion from being established.

Here we report results from a much longer simulation covering the period January 1985–April 1996, obtained with a new model developed recently as a tool to study the general circulation of the ocean. Model formulation and numerical implementation are described in detail by Marshall *et al.*¹¹. For the present purpose the model was configured on a 1° grid with realistic topography over the latitude range ±80°, and with 20 levels in the vertical with layer thickness ranging from 25 m at the surface to 500 m at depth¹². The model was started from the final state of a previous 3-year spin-up run, and driven by 12-hourly wind stress fields and daily fields of surface heat and freshwater fluxes from the National Centers for Environmental Prediction (NCEP) for the period 1985–96. In addition to the surface heat and freshwater fluxes, the model was relaxed towards monthly mean sea surface temperature (SST) fields (that served as the lower boundary condition in the NCEP analyses) and towards monthly Levitus *et al.*¹³ salt climatology. The relaxation coefficient was varying in space and time and represented an estimate of the sensitivity of the surface flux to the SST¹⁴. Ice was simulated by a thermodynamic ice model¹⁵ and biharmonic friction was applied to the momentum equations. Forcing by barometric pressure is not included, but for periods analysed here (longer than 10 days), the inverted barometer approximation should hold¹⁰. A detailed description of the model solution cannot be given here, but overall the model performs satisfactorily on the large scale when compared to observations^{12,16}.

To examine the effects of the ocean on polar motion excitation, we follow the formulation of Barnes *et al.*⁵ and calculate effective equatorial angular-momentum functions χ_1^O and χ_2^O (Fig. 1). Each χ includes a motion term due to changes in the velocity field (χ^V), and a mass term due to changes in bottom pressure (χ^P). The motion

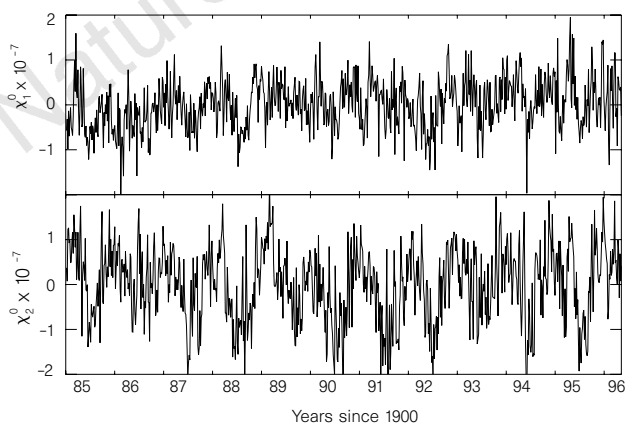


Figure 1 Five-day averaged values of χ_1^O and χ_2^O for the period January 85–April 96. Means have been removed. χ_1^O and χ_2^O are dimensionless and essentially proportional to the oceanic angular momentum about the two equatorial axes, conventionally taken to point towards the Greenwich and 90°E meridians, respectively⁵. The functions incorporate effects of the elasticity of the Earth and thus represent the effective excitation of polar motion by the oceans¹⁵. The time series show a rich variability over a wide range of timescales, and with no significant long term trends. The seasonal cycle is most conspicuous in χ_2^O , which tends to have slightly larger amplitudes than χ_1^O .

and mass terms were evaluated for the more than 11 years of model output, using 5-day averages of the velocity and bottom pressure fields, respectively. Bottom pressure was calculated based on the hydrostatic relation, using sea level and density estimated by the model, with the sea level corrected by a spatially constant, but time-variable, factor accounting for overall volume changes due to steric effects¹⁷. Both variable circulation and mass fields contribute to the oceanic excitation series, but there is more power in the pressure terms over most frequencies (Fig. 2), particularly in χ_2^P , a finding also characteristic of previous results from other models^{9,10}.

Corresponding time series for the effective atmospheric equatorial angular-momentum functions, χ_1^A and χ_2^A , based on the NCEP/NCAR (National Center for Atmospheric Research) reanalysis products, were obtained from the Sub-Bureau for Atmospheric Angular Momentum of the International Earth Rotation Service (IERS)¹⁸. Atmospheric χ^V included winds integrated up to the 10-mbar pressure level, and χ^P were based on the inverted barometer approximation¹⁸, consistent with our ocean modelling assumptions. Equivalent polar motion excitation functions, χ_1^G and χ_2^G , were computed from the EOP 97 C 04 pole positions reported by IERS, using the method of Wilson¹⁹. Five-day averaged time series were created from the original series to be consistent with the ocean products.

Comparison of the frequency spectra for χ^O and χ^A (Fig. 3) indicates that, although in general weaker than the atmosphere (the total power in χ_1^O and χ_2^O amounts to 70% and 32% of that in χ_1^A and χ_2^A , respectively), the oceans are a non-negligible source of polar motion over most frequency bands. Particularly important seem to be the seasonal signals in χ_1^O . Furthermore, the power density for the combined oceanic and atmospheric time series, χ^{O+A} , is consistently higher than χ^A alone across the entire spectrum (with the exception of the seasonal band for χ_2) and generally closer to the observed levels of polar motion excitation (χ^G). We note that for the seasonal band in χ_2 , atmospheric excitation is above what is observed. The addition of the oceanic excitation decreases the seasonal χ_2 power

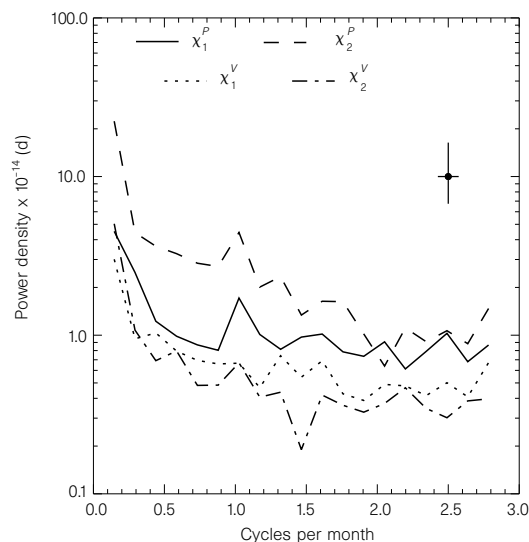


Figure 2 Power spectral density for oceanic χ_1^P (solid line), χ_1^V (dotted), χ_2^P (dashed) and χ_2^V (dotted-dashed) calculated by averaging respective periodograms over 20 adjacent frequencies. 95% confidence limits based on 40 degrees of freedom are shown on the upper right (vertical bar), together with the bandwidth (horizontal bar). The lowest frequency shown corresponds essentially to the seasonal band, including periods between 13.7 and 4.6 months. The differences between the various χ spectra reflect in part the particular choice of equatorial axes and the way oceanic variability projects on the spatially varying factors involved in each χ (refs. 1, 5). Regional contributions to the global integral represented by the χ^O values will be reported elsewhere.

density so that, over all bands, the power density in combined ocean–atmosphere excitation is below χ^G levels. Although the differences for each band are within the noise level, they could be made formally significant with further averaging in frequency. Therefore, the importance of other sources of excitation cannot be ruled out.

Besides contributing significant power to that available from atmospheric excitation alone, the inclusion of the oceanic series leads to significantly improved coherence with the observed polar motion excitation, for the frequency bands resolved (Fig. 3). Coherence amplitudes are consistently larger in the case of the joint atmosphere–ocean excitation, and phases are closer to zero, as expected for an improved agreement between geophysical excitation and observed polar motion. It is worth noting the case of the seasonal band for χ_1 , for which the addition of the oceans increases the coherence amplitude by 0.5, bringing it above the significance level and improving significantly the phase estimate. Overall, the correlation coefficients increase from 0.53 and 0.60 for the pairs (χ_1^A, χ_1^G) and (χ_2^A, χ_2^G) to 0.84 and 0.72 for the pairs (χ_1^{O+A}, χ_1^G) and (χ_2^{O+A}, χ_2^G) , respectively, and the root-mean-square difference between the paired series is reduced by $\sim 14\%$.

The present data (covering >11 years) are sufficient to separate the annual and Chandler periods (the latter is estimated¹ at 433 days) using harmonic analysis, but it is still too short a record to provide sufficient spectral resolution near those frequencies. Nevertheless, the amplitudes and phases of the harmonics at those periods (not shown) point to similar conclusions: the joint ocean–atmosphere excitation compares substantially better with the observed excitation at these periods than when only the atmosphere is considered. Determining with more certainty whether the excitation by the two geophysical fluids suffices to explain polar motion at these specific periods will require a longer record.

Even without considering the ocean's role, the presented coherence and correlation between χ^A , calculated from the NCEP/NCAR reanalysis, and χ^G , based on the recently created IERS data set,

represent an improvement over results from previous studies^{2,20,21}. The quality of the atmospheric and geodetic time series have, thus, considerably improved in recent years. With the inclusion of the oceanic signals, we are now approaching levels of agreement with χ^G much sought over the past decade, and similar to those obtained for the length of day²².

The ocean results reported here stem from modelling alone, without any estimation of the ocean circulation and mass fields by constraining the model to data. Nevertheless, the present significant improvements in the agreement with the observed polar motion, obtained when the simulated oceanic effects are added to the atmospheric excitation, attest to the high quality of the ocean model and its atmospheric surface forcing fields. The present study thus provides an unprecedented measure of consistency between three vastly different, but intimately coupled, dynamical systems, being modelled and observed at quite different levels of complexity. It also emphasizes the importance of the ocean in the Earth system, and the necessity to consider the effect of the ocean in Earth-related studies, including the planet's angular-momentum budget as well as fluctuations in the geoid.

Present simulations of the ocean excitation parameters are undoubtedly not free from error. Improved estimates of the oceanic χ functions are expected to come from efforts to incorporate available oceanic data in the estimation process, which are currently underway, as well as improvements in model physics and formulation, and forcing fields¹⁶. In particular, the inclusion of pressure forcing will probably be important¹⁰ as the scope of inquiry is extended to weekly and daily timescales. At these periods, accurate representation of the coupling forcing fields acting at the ocean–atmosphere interface will be crucial. \square

Received 27 June; accepted 27 October 1997.

1. Eubanks, T. M. in *Contributions of Space Geodesy to Geodynamics: Earth Dynamics 1–54* (eds Smith, D. & Turcotte, D.) (AGU Monogr., Geodynamics Ser., Vol. 24, Am. Geophys. Un., Washington DC, 1993).
2. Eubanks, T. M., Steppe, J. A., Dickey, J. O., Rosen, R. D. & Salstein, D. A. Causes of rapid motions of the Earth's pole. *Nature* **334**, 115–119 (1988).

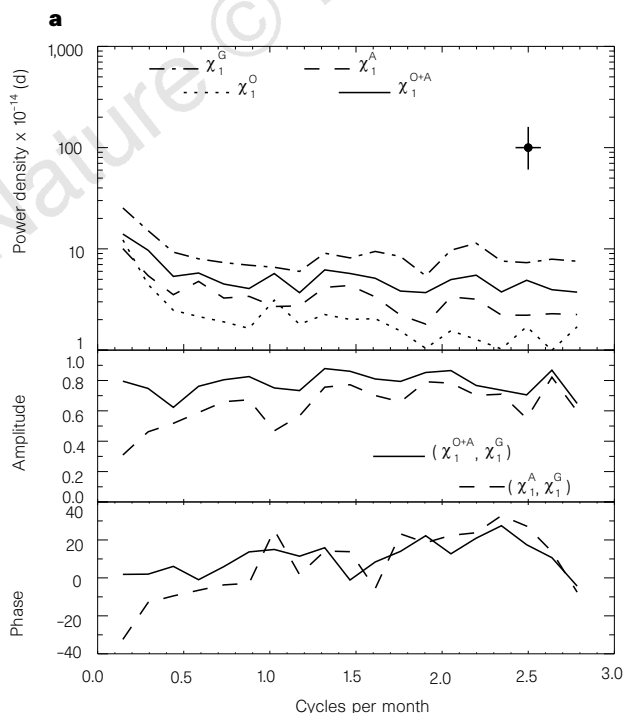
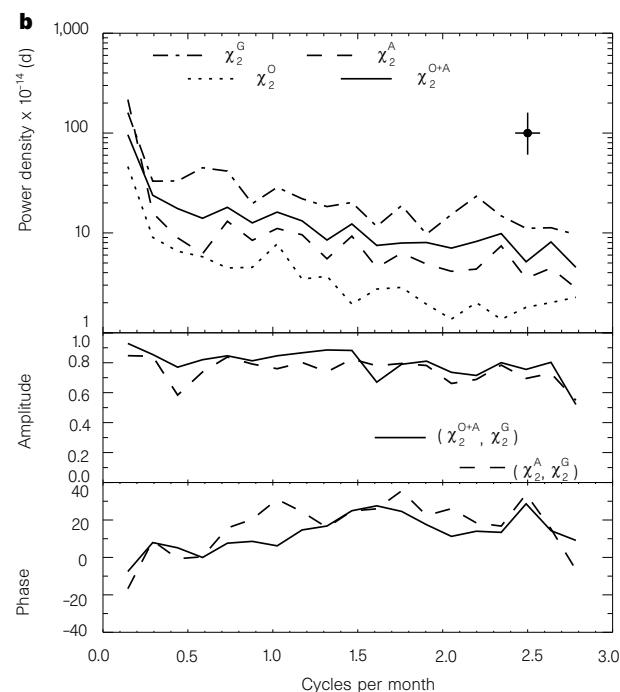


Figure 3 Assessment of oceanic effects on the excitation of polar motion. **a**, Power spectral density of χ_1^O , χ_1^A , χ_1^{O+A} , χ_1^G and coherence amplitude and phase in degrees for the pairs (χ_1^A, χ_1^G) and (χ_1^{O+A}, χ_1^G) . Similar curves for χ_2 series are shown in **b**. Power spectral density and coherence are calculated with band-averaging



over 20 frequencies. 95% confidence limits for the spectra are shown on the upper right (vertical bar), together with the bandwidth (horizontal bar). Coherence amplitudes >0.38 are significantly different from zero at the 95% confidence level.

3. Gross, R. S. & Lindqwister, U. J. Atmospheric excitation of polar motion during the GIG '91 measurement campaign. *Geophys. Res. Lett.* **19**, 849–852 (1992).
4. Chao, B. F. Excitation of Earth's polar motion by atmospheric angular momentum variations, 1980–1990. *Geophys. Res. Lett.* **20**, 253–256 (1993).
5. Barnes, R. T. H., Hide, R., White, A. A. & Wilson, C. A. Atmospheric angular momentum fluctuations, length-of-day changes and polar motion. *Proc. R. Soc. Lond. A* **387**, 31–73 (1983).
6. Wilson, C. R. & Haubrich, R. A. Meteorological excitation of the Earth's wobble. *Geophys. J. R. Astron. Soc.* **46**, 707–743 (1976).
7. Wahr, J. M. The effects of the atmosphere and oceans on the Earth's wobble and on the seasonal variation in the length of day—II. Results. *Geophys. J. R. Astron. Soc.* **74**, 451–487 (1983).
8. Salstein, D. A., Ponte, R. M., Rosen, R. D. & Cady-Pereira, K. Angular momentum in a free-surface ocean general circulation model. *Eos (Spring Meeting Suppl.)* **76**, 82 (1995).
9. Bryan, F. O. & Smith, R. D. Oceanic excitation of variations in Earth rotation from a high resolution global model. *Eos (Fall Meeting Suppl.)* **76**, 61 (1995).
10. Ponte, R. M. Oceanic excitation of daily to seasonal signals in Earth rotation: results from a constant-density numerical model. *Geophys. J. Int.* **130**, 469–474 (1997).
11. Marshall, J., Adcroft, A., Hill, C., Perelman, L. & Heisey, C. A finite-volume, incompressible Navier Stokes model for studies of the ocean on parallel computers. *J. Geophys. Res.* **102**, 5753–5766 (1997).
12. Marshall, J., Hill, C., Perelman, L. & Adcroft, A. Hydrostatic, quasi-hydrostatic and non-hydrostatic ocean modeling. *J. Geophys. Res.* **102**, 5733–5752 (1997).
13. Levitus, S., Burgett, R. & Boyer, T. *World Ocean Atlas 1994* Vol. 3, *Salinity* and Vol. 4, *Temperature* (NOAA Atlas NESDIS 3 and 4, US Dept of Commerce, Washington DC, 1994).
14. Barnier, B., Siefridt, L. & Marchesiello, P. Thermal forcing for a global ocean circulation model using a three-year climatology of ECMWF analyses. *J. Mar. Sys.* **6**, 363–380 (1995).
15. Jayne, S. & Marotzke, J. A destabilizing thermohaline circulation—atmosphere—sea ice feedback. *J. Clim.* (submitted).
16. Stammer, D. *et al.* *The Global Ocean Circulation Estimated from TOPEX/POSEIDON Altimetry and the MIT General Circulation Model* (Rep. 49, MIT Center of Global Change Science, Cambridge, 1997).
17. Greatbatch, R. J. A note on the representation of steric sea level in models that conserve volume rather than mass. *J. Geophys. Res.* **99**, 12767–12771 (1994).
18. Salstein, D. A., Kann, D. M., Miller, A. J. & Rosen, R. D. The sub-bureau for atmospheric angular momentum of the international earth rotation service: a meteorological data center with geodetic applications. *Bull. Am. Meteor. Soc.* **74**, 67–80 (1993).
19. Wilson, C. R. Discrete polar motion equations. *Geophys. J. R. Astron. Soc.* **80**, 551–554 (1985).
20. Salstein, D. A. Monitoring atmospheric winds and pressures for Earth orientation studies. *Adv. Space Res.* **13**, 11175–11184 (1993).
21. Salstein, D. A. & Rosen, R. D. in *Proc. 7th Conf. on Climate Variations 344–348* (Am. Meteor. Soc., Boston, 1997).
22. Rosen, R. D. The axial momentum balance of Earth and its fluid envelope. *Surv. Geophys.* **14**, 1–29 (1993).

Acknowledgements. We thank D. Spiegel for help with the computation, and F. Bryan, B. Chao, R. Rosen and D. Salstein for comments. This work was supported by NASA's Mission to Planet Earth.

Correspondence and requests for materials should be addressed to R.M.P. (e-mail: ponte@aer.com).

High hunting costs make African wild dogs vulnerable to kleptoparasitism by hyaenas

Martyn L. Gorman*, Michael G. Mills†, Jacobus P. Raath† & John R. Speakman*

* Department of Zoology, University of Aberdeen, Tillydrone Avenue, Aberdeen AB24 2TZ, UK

† National Parks Board, Kruger National Park, Box X402, Skukuza 1350, Republic of South Africa

The African wild dog *Lycaon pictus* is critically endangered, with only about 5,000 animals remaining in the wild¹. Across a range of habitats, there is a negative relationship between the densities of wild dogs and of the spotted hyaena *Crocuta crocuta*². It has been suggested that this is because hyaenas act as 'kleptoparasites' and steal food from dogs. We have now measured the daily energy expenditure of free-ranging dogs to model the impact of kleptoparasitism on energy balance. The daily energy expenditures of six dogs, measured by the doubly labelled water technique, averaged 15.3 megajoules per day. We estimated that the instantaneous cost of hunting was twenty-five times basal metabolic rate. As hunting is energetically costly, a small loss of food to kleptoparasites has a large impact on the amount of time that dogs must hunt to achieve energy balance. They normally hunt for around 3.5 hours per day but need to increase this to 12 hours if they lose 25% of their food. This would increase their sustained metabolic scope to a physiologically unfeasible twelve times the basal metabolic rate. This may explain why there are low populations of wild dogs in regions where the risk of kleptoparasitism is high.

African wild dogs are medium-sized carnivores (weighing ~25 kg) that live in packs of 4–20 adults and their dependent young. They feed predominantly on ungulates weighing 15–100 kg which they hunt and kill cooperatively. The members of a pack are normally nomadic within a large (~500 km²) home range. Wild dogs were formerly widespread south of the Sahara, but fewer than 5,000 individuals now survive¹. This serious decline in numbers has been blamed on several factors including habitat loss, persecution by humans³ and the transfer from domestic dogs of diseases such as rabies⁴. African wild dogs, however, live at low densities even in large areas of relatively undisturbed habitat, and their biomass is generally one to two orders of magnitude lower than that of competing spotted hyaenas². Across a range of habitats, there is a negative relationship between the density of dogs and hyaenas. Where the population density of hyaenas is high, and where visibility is good, for example on the Serengeti plains, these animals accumulate at the kills of dogs and reduce the dogs' rate of food intake^{5,6}. Hyaenas rarely take food from dogs in heavily wooded areas such as the Selous or Kruger Park, however^{7,8}. It is claimed that kleptoparasitism by hyaenas has been part responsible for the decline, or even demise, of wild-dog populations in open habitats⁹.

We used the doubly labelled water (DLW) technique¹⁰ to measure the daily energy expenditures (DEEs) of six fully grown dogs (three males and three females) from a pack living in the southwest of the Kruger National Park, Republic of South Africa. The pack consisted of 5 adults, 16 yearlings aged 16 months, and 27 pups aged 3–4 months. In the Kruger National Park, dogs generally hunt early in the morning and again towards dusk. At the time of the study, the dogs were away from the den and hunting for a total of 207 ± 15.1 min per day (mean ± 95% confidence interval (CI); n = 59 days). They spent the remainder of the day at rest. Daily energy expenditure, measured by DLW, averaged 15.3 MJ (Table 1). This is equivalent to a food intake of 3.5 kg of ungulate meat per day, assuming an energy content of 5.2 MJ per kg wet weight, a digestive efficiency of 93% and a 10% loss of energy in the urine. This figure agrees well with field determinations of rates of food intake, which range from 2.5 to 3.5 kg per dog^{7,8}. The high variability in DEEs among the six dogs probably reflects day-to-day variation in the involvement of individuals in the group hunt. As the study pack consisted of only 5 adults, together with 27 dependent pups and 16 yearlings who had just reached the age at which wild dogs hunt effectively, the pack might have been hunting rather more intensely than packs with a more favourable ratio of adults to young.

For comparison, allometric equations¹¹ predict a DEE of 6.0 MJ per day for a moderately active 25-kg domestic dog and 6.7 MJ per day for a highly active individual. The field metabolic rate of a 25-kg eutherian mammal has been predicted to be ~12.6 MJ per day¹². Measurements of food intake by working border collies¹³ give a value of 8.2 MJ per day for a 25-kg dog active for 6 hours per day. Alaskan sledge dogs weighing 25 kg used 47 MJ per day, as measured by both the DLW technique and the rate of food intake, on a 70-hour, 490-km sledge race across Arctic Canada¹⁴. By these comparisons, African wild dogs appear to be working extremely hard, despite the fact that they are active for only 3.5 hours per day. Moreover, the predicted basal metabolic rate (BMR) for a 25-kg dog

Table 1 Daily energy expenditures of six African wild dogs measured using the doubly labelled water technique

Dog	Sex	Mass (kg)	Plateau estimate (kJ per day)	Intercept estimate (kJ per day)
1	F	24	8,043	7,223
2	F	25	8,729	7,732
3	F	23	16,686	15,716
4	M	27	18,252	17,910
5	M	27	20,281	19,362
6	M	25	19,806	18,729